J Nanostruct 12(4): 948-958, Autumn 2022

RESEARCH PAPER

Using SWCNTs to Enhancing the Performance of P3HT:PCBM-Based Organic Solar Cells

Mohammed K. Al Hashimi [1], Buraq T. SH. AL-Mosawi [1], Burak Y. Kadem [2], and Yaqub Rahaq [3]*

[1] *Department of Physics, College of, Education, University of Misan, Misan, Iraq*

[2] *Department of Renewable Energies, College of Science, Al- Karkh University for Science, Baghdad, Iraq*

[3] *Material and Engineering Research Institute, Sheffield Hallam University, Sheffield, UK*

ARTICLE INFO

Article History:
Received 27 June 2022
Accepted 16 September 2022
Published 01 October 2022

Keywords:
P3HT
PCPM
SEM
Solar cell
SWCNTs
XRD

ABSTRACT

The study shows how the solution processed bulk-heterojunction solar cells can exhibit better performance on the basis of a low-bandgap polymer combined with a fullerene derivative. Co-solution is used to blend the dopant single-walled carbon nanotubes (SWCNTs) with poly (3-hexyl thiophene) (P3HT) and [6,6]-phenyl-C61-butyric acid methyl ester (PCBM) at 0% to 1% concentrations. We use Carrier mobility measures to show that an increase in doping concentration causes an increase in hole conductivity and mobility. This was shown in the XRD studies and established through the absorbance spectra that shows the specific 600 nm shoulder. The study demonstrates that it is possible to improve the open circuit voltage and short circuit current of the relevant solar cells by doping at a concentration of 0.5%, which leads to increased power conversion efficiencies. The improvement in performance is explained with respect to trap filling because of the higher carrier density and lower recombination that is associated with better mobility.

How to cite this article
Al Hashimi M K., AL-Mosawi B T S. , Kadem B Y., Rahaq Y. Using SWCNTs to Enhancing the Performance of P3HT:PCBM-Based Organic Solar Cells. J Nanostruct, 2022; 12(4):948-958. DOI: 10.22052/JNS.2022.04.016

INTRODUCTION

Organic photovoltaic (OPV) devices created on the basis of electron-donating conjugated polymers and electron accepting fullerene derivatives are most likely to be used as low-cost and flexible renewable sources of energy in the last few years [1-3]. Polymer absorbs the light that is incident on the devices and excitons are created on the polymer chains [4, 5]. Thereafter, there is diffusion of these excitons to the polymer-fullerene interface, and here they separate into electron and hole, with the standard diffusion length being around 10 nm [5]. The composite of poly (3-hexyl thiophene) (P3HT) and [6,6]-phenyl-C61- butyric acid methyl ester (PCBM) is the most effective OPV material employed, and it is not utilized as the model system, having accomplished good efficiencies with solar illumination [6,7]. Because of their unique charge transport features and electron acceptor behaviour, carbon nanotubes (CNT) have been recently included in the OPVs by doping them into the P3HT:PCBM photoactive layer so that they can be used. The two single walled carbon nanotubes (SWCNTs) have been included in photoactive materials to improve device performance [8-13]. Electron mobility is

* *Corresponding Author Email: mr.mohammed@uomisan.edu.iq*

increased substantially by incorporating nanotubes in the photoactive layer, which decreases the recombination rate and brings about an improvement in the OPV device performance. The compatibility of distinct stages in the photoactive layer is a major issue with these devices, mainly of the nanotubes that cannot dissolve in majority of the solvents utilized to create the devices. Since the nanotubes have low solubility, they server as the key obstacle in achieving consistent combinations of polymer/fullerene/nanotubes that make the devices exhibit low performance. To overcome this issue, nanotubes can be functionalized using appropriate reagents that increase the dispersibility of functionalized product in organic solvents [14–15]. Since the SWCNTs have low production cost and are easily available, they are increasingly used in OPV devices. The chemical functionalization causes nanotube bundles to exfoliate, which enhances processability and solubility. The chemical and physical attributes of nanotubes are altered by the functionalization, thus enhancing the interaction among the nanotubes and polymer [16]. The greatest power conversion efficiency achieved by doping functionalized SWCNTs to P3HT /PCBM was 2.5% of less than AM1.5 illumination [17]. When these functionalized adducts were included in P3HT / PCBM OPV devices in varied doping concentrates, better performance was exhibited in comparison to standard devices. The functional groups were selected in a way that they are likely to generate highly percolation networks with P3HT and PCBM. In addition, as these adducts have higher solubility, improved blends with P3HT as well as PCBM are created, which leads to a decrease in exciton dissociation pathway and improved device performance [18] .

MATERIALS AND METHODS

Materials

The Chemical Vapor Deposition (CVD) technique was used to grow single-walled carbon nanotubes (SWCNTs) (diameter of 0.7–1.4 nm). Titanium dioxide (TiO_2), poly (3-hexyl thiophene) (P3HT), [6,6]-phenyl-C61-butyric acid methyl ester (PCBM), Indium tin oxide (ITO), chlorobenzene and Powder sample of Vanadium Oxide V_2O_5 were bought from Sigma Aldrich.

Organic Solar Cell Preparation

PCBM and P3HT were dissolved to chloroform or chlorobenzene in a ratio of 1:1 and were mixed for 1 hour at a temperature of 60 °C. The SWCNTs were dispersed to a 1:3 mixture of nitric acid and sulphuric acid, after which it was sonicated

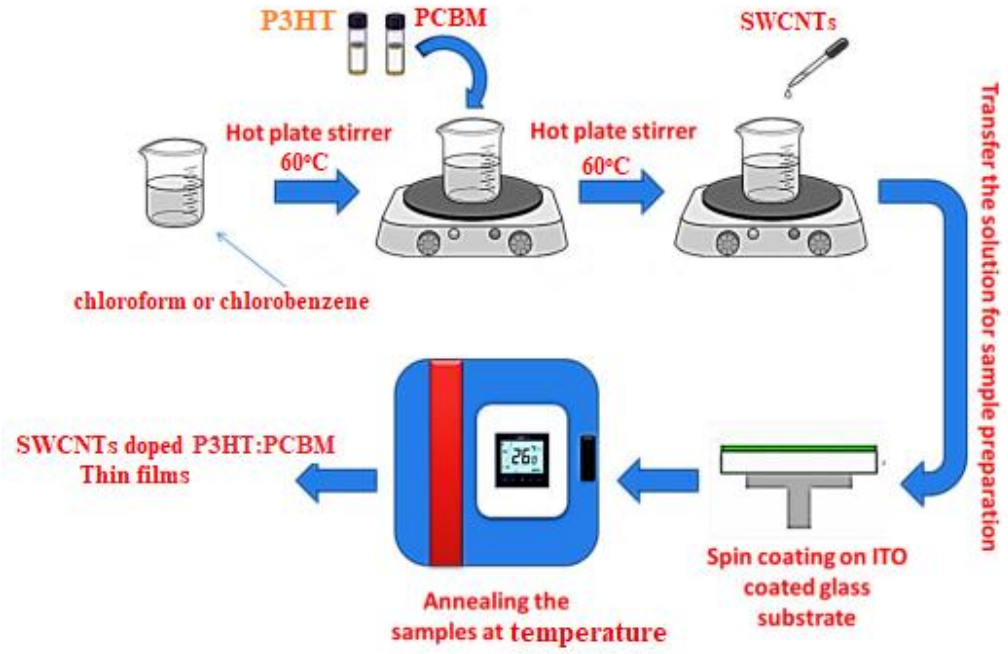

Fig. 1. Steps of preparing P3HT:PCBM:SWNTs thin films.

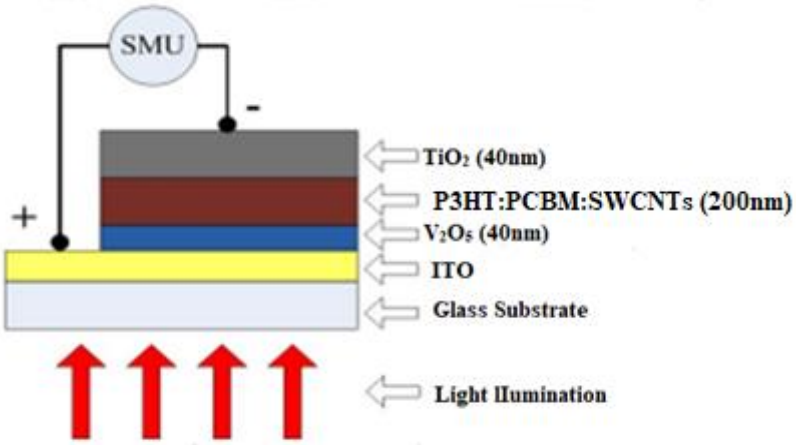

Fig. 2. The structure the fabricated organic solar cell.

at a temperature of 50 °C for 1 hour to remove impurities and to create shortened SWCNTs having terminal COOH groups. Water was added to the solution obtained to dilute it, after which it was centrifuged at 6000 rpm for 2 hours to eliminate large aggregates. A polytetrafluoroethylene membrane having a pore size of 200 nm was used to filter the supernatant. The remaining particles were carefully washed with water by decantation to eliminate any leftover acid, after which they were dried in an oven at a temperature of 100 °C. The solid sample of acid obtained following treatment with SWCNTs was added to chlorobenzene or chloroform and sonicated for 1 hour at 60 °C. Subsequently, Fig. 1 illustrates the steps of preparing SWCNT solution was added to the (P3HT: PCBM) solution in varying volumes and sonicated for 1 hour. The photovoltaic devices identified in Fig. 2 were constructed on 25mm×25 mm indium–tin-oxide (ITO) glass substrates, having a sheet resistance of 8–12 Ω sq^{-1}. V_2O_5, being a buffer layer, was mixed in 5 ml acetonitrile to create a solution where there was a 1:50 weight ratio for V_2O_5: acetonitrile. A magnetic bar on a hot plate was used to mix this V_2O_5 solution at a temperature of 60°C for 1 hour. It was then spin cast from a solution on the ITO substrate, providing a thickness of 40 nm layer on average, after which it was baked for 3 hours at 100 °C within a nitrogen-filled glove box. To deposit the photoactive layer, a mixture of P3HT:PCBM:SWCNTs was spin-coated at an optimal ratio of 1:1:0.5 added to chlorobenzene or chloroform at 1000 rpm for 60 seconds, which created films with thicknesses of 200 nm. After drying the films for 1 hour at room temperature, they were annealed for 30 more minutes at a temperature of 80 °C in nitrogen. The TiO_2 layer that was earlier created over the P3HT:PCBM:SWNTs active layer, after which it was annealed at hot plate within the nitrogen filled glove box at a temperature of 120 °C for 10 minutes, which created films with thicknesses of 40 nm. . Thermal evaporation of aluminum cathodes was finally achieved using a shadow mask. An Agilent B1500A semiconductor device analyzer was used to carry out current–voltage (I–V) measurements at room temperature. To achieve photovoltaic characterization, the cells were illuminated with 100mW cm^{-2} power intensity of white light using an Oriel solar simulator (active area ~5 mm^2) that had an AM1.5 filter across the glass/ITO side. Right after the creation of device, all measurements were instantly carried out in air.

Characterizations

An X'Pert Philips X-ray diffractometer (MPD), nanoscope IIIa multimode AFM (BrukerAFM) and scanning electron microscope (FEINova SEM) were used to analyze the structure and morphology of all thin films of SWCNT-doped P3HT: PCBM. The optical characterization of these thin films was achieved using UV-visible spectroscopy at a wavelength range of 190–1100 nm. M200 spectroscopic ellipsometer created by J. A. Woollam Company was used to determine the thin film thickness parameter at (370-1000) nm wavelength. The 4200 Keithley Semiconductor characterization system (SCS) was used to test the solar cells electrically (photovoltaic properties). Intensity of 100 mW/cm^2 was created using AM

1.5 irradiation of the solar simulator.

RESULTS AND DISCUSSION

Morphological Properties

The AFM and SEM doped and undoped P3HT:PCBM films micrographs along with the disparate content of the SWCNT doping element are shown in Fig. 3. The concentration of SWCNT doping has an impact on the surface morphology of P3HT:PCBM films. The figure presents the AFM images of the P3HT:PCBM and P3HT:PCBM:SWCNT layers with different concentrations of SWCNT doping, i.e. 0.5% and 1wt%. The SWCNT concentration seems to have an impact on the surface morphology, when the surface root mean square (RMS) roughness values are 1.9, 2.679 and 2.189, respectively. There will be an increase in the density of the P3HT:PCBM layer with doping 1 wt% of SWCNTs, which will be evenly spread out on the surface. Hence, the film surface was flatter [16]. Fig. 3 shows the AFM, and it can be seen that there is a rougher surface morphology of the film with 0.5% concentration of SWCNTs. An identical phenomenon was seen in P3HT:PCBM:SWCNT layers with different SWCNT concentrations, depicting that the SWCNT loading amount causes an increase in phase separation and aggregation of nanoparticles [19-21]. There is an increase in phase segregation with the contact area between the aggregating particles increasing. Table 1. presents a summary of the findings.

The extensive structure of SWCNTs was confirmed by examining SEM image of polymer samples. The results make it evident that the SWCNTs are scattered with tangled hairs in the polymer layer with doping at 1% SWCNT [22]. The P3HT:PCBM film with 0.5% at SWCNTs concentration doping depicts a rough surface. In addition, it was noted that improved dispersion is shown by SWCNT incorporated active layers. A random distribution of localities demonstrating SWCNT distribution is also seen [23,24].

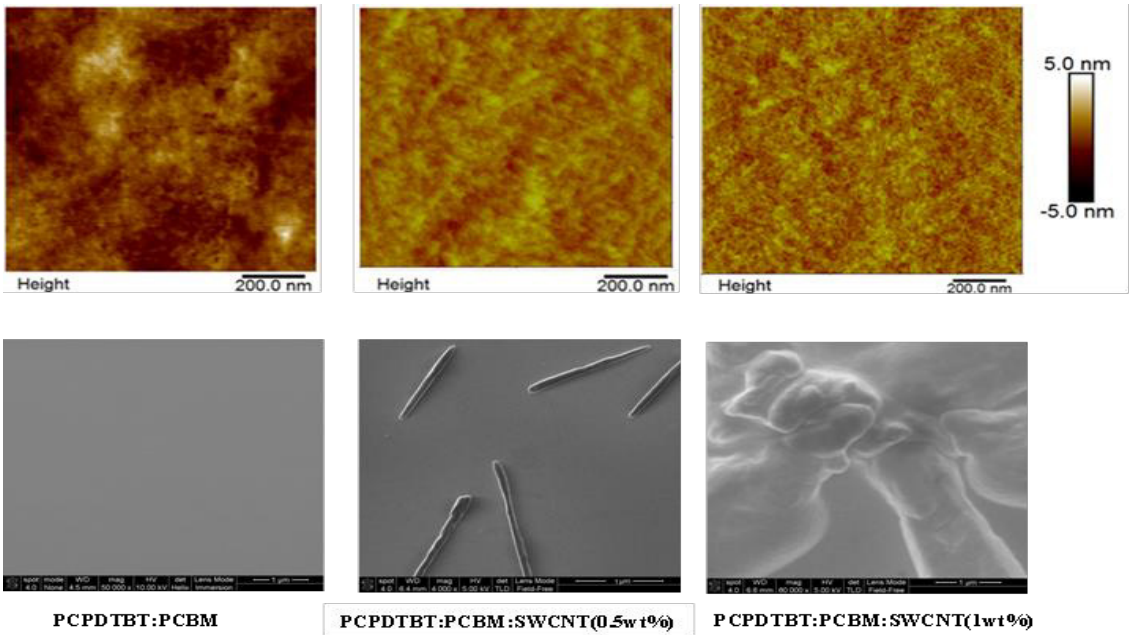

Fig. 3. The AFM and SEM images of P3HT:PCBM films with different concentrations of SWCNT doping .

Table 1. AFM data for the P3HT:PCBM doping with different ratio of SWCNT

Different doping	RMS roughness (nm)
Pure	1.984
0.5%	2.679
1%	2.189

X-ray of P3HT:PCBM doping with SWCNT

The X-rays of P3HT:PCBM, P3HT:PCBM:0.5%SWCNTs, and P3HT:PCBM:1%SWCNTs layers are shown in Table 2. and Fig. 4, respectively. The appearance of a crystallization can be observed, which happens because of the inclusion of the SWCNTs that produces the crystallization of composites P3HT:PCBM and increases the order in the matrix. It is typically seen in the π-π stacking among benzene rings and it has been found to enhance polymer crystallization in the composite films [25,26].

Absorbance Spectrum Of P3HT:PCBM With Different Doping SWCNT

Optical absorption spectra for P3HT:PCBM doped with SCWNTs at 0, 0.5 & 1 wt% concentrations are shown in Fig. 5, respectively. The films employed for absorption measurements are controlled so that they are approximately of the same thickness (200nm). It is shown by the absorption of different P3HT:PCBM doped with varying SWCNT concentrations that the inclusion of SWCNTs enhances absorption of the P3HT:PCBM [21]. There is absorption of SWCNTs and the blend polymer in the infrared and visible areas, correspondingly. Consequently, there is considerably higher absorption of the blend. Furthermore, it is shown by the absorption of the blend that a particular structuring is caused by the polymer, as can be seen by existence of fine structures [27]. The absorption maximum of P3HT:PCBM films peaks is approximately 488nm. There is a change in the absorption spectrum with the doping of SWCNT with P3HT:PCBM blend: the

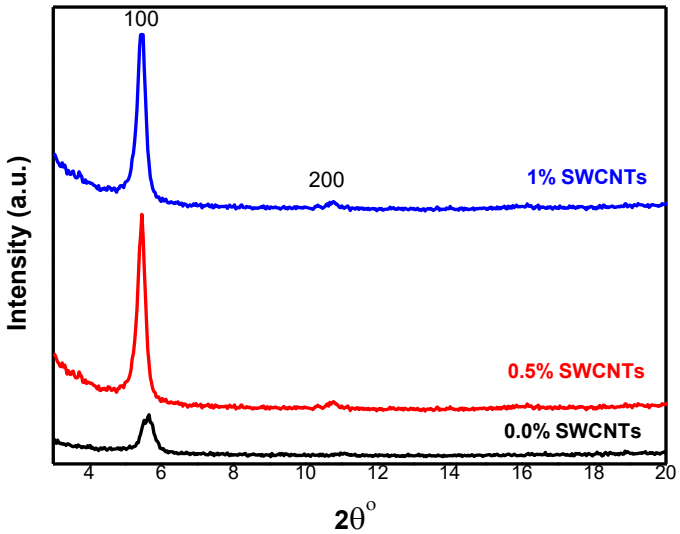

Fig. 4. XRD patterns of P3HT:PCBM films with different concentrations of SWCNT doping .

Table 2. XRD data for the P3HT:PCBM doping SWCNTs.

Annealing C	Mille Indices (hkl)	Angle (2θ) Degree	Angle (2θ) degree	d values (A)	d values (A)	FWHM Degree	D_{hkl} Nm
		Observed	Stander	Observed	Stander		
	100	5.39660	5.504	1.8502	1.7965	0.5523	15.053
Pure	200	10.77174	10.621	1.7974	1.7652	0.9957	8.3753
	100	5.40524	5.504	1.8200	1.7965	0.4897	16.6718
0.5%	200	10.77174	10.621	1.7974	1.7652	0.9944	8.3863
	100	5.40110	5.504	1.8252	1.7965	0.7774	10.6894
1%	200	10.77174	10.621	1.7974	1.7652	0.9957	8.3652

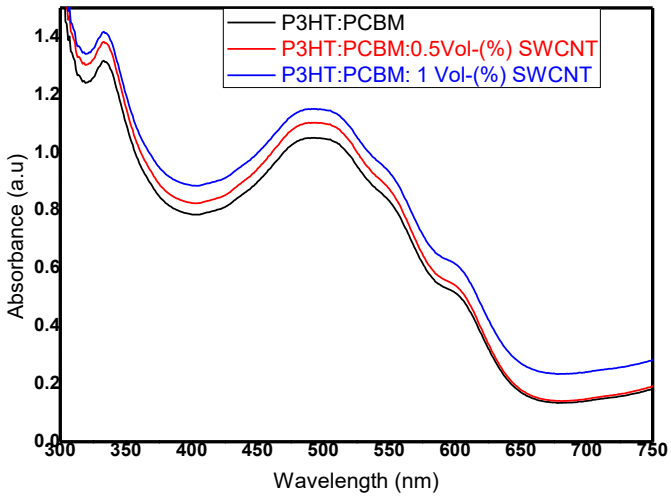

Fig. 5. UV–vis absorption spectra of P3HT:PCBM with different concentrations of SWCNT doping .

absorption intensity increases and the shoulder appears at 550 and 630 nm, with the absorption maximum being displaced to 500 nm. This increase in absorption intensity may be explained by the structuring of the polymeric chains surrounding the carbon nanotubes [28]. These findings are consistent with those of the studies carried out in the past [29]. There is an increase in the shoulder noted at 600nm in the P3HT:PCBM blend with the inclusion of SWCNT. This is because of the partial crystallization of the conjugated polymer because the SWCNTs and the polymer interact with each other [30]. Therefore, the absorption intensity increased with the higher production of electron-hole pairs by the SWCNTs that leads to better power conversion efficiency [29].

Carrier Mobility Measurement

The carrier mobility of SWCNT: P3HT:PCBM composite films was determined using the space charge limited current (SCLC) technique [31].

The Mott-Gurney law may be used to quantitatively determine the carrier mobility of every device:

$$J = \frac{9}{8}\varepsilon_r \varepsilon_0 \mu \frac{V^2}{L^3}$$

Here, refers to the relative dielectric constant, signifies the permittivity of the free-space, denotes the charge carrier mobility, while L is the device thickness. The estimated electron and hole mobility ($_e$ and $_h$) with the relative dielectric constant of PCBM is fixed at 3.9 [32], while that of P3HT is fixed at 3.2 and of P3HT:PCBM at 3.4 [33]. These are presented in Fig.s 6 and Table 3. It can be seen that the electron-only and hole-only device pair with 0.5 wt% SWCNTs had an appropriately matching $_e$ and $_h$ of 9.593 x 10^{-6} m^2 V^{-1} S^{-l} , 8.756 X 10^{-6} m^2 V^{-1} s^{-1}, respectively, and the mobility values achieved were 1.87 x 10^{-5} $m^{-2}V^{-1}s^{-1}$ and 2.37 x 10^{-5} $m^{-2}V^{-1}s^{-1}$ correspondingly for P3HT:PCBM without and with SWCNTs, that is highly desired to achieve high performance of optoelectronic devices [34]. It is suggested that the improvement noticed in the photocurrent is essentially because the electron transport is highly efficient across the nanotube percolation pathways. There is dissociation of the photogenerated excitons in the reference device at the P3HT:PCBM interfaces, and the electrons hop over the fullerenes to shift to the Au. When the nanotubes are included in the photoactive layer, more paths are provided to the electrons across the distributed carbon nanotube percolation network, which restrains charge recombination and improves electron transport. It is believed that for larger concentrations of 1.0 wt% SWCNTs, the photocurrent is restricted by greater recombination rate, and the effective mobility is decreased because of the SWCNTs [35]. When the SWCNT concentration is increased, the SWCNTs will possibly be aligned parallel to one other and come together in the crystalline ropes because of the powerful intertube van der Walls attraction. Because of the greater trapping

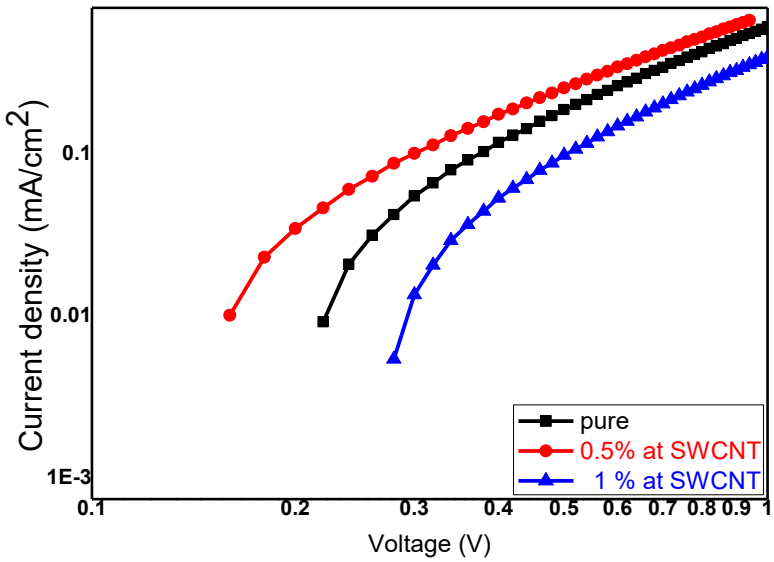

Fig. 6. The slope of J-V characteristics with logarithmic scales of an ITO/ V_2O_5 / P3HT:PCBM/ TiO_2 /Au device with various concentration of SWCNT.

Table 3. Electron motilities of PCBM based electron-only devices, hole mobilities of P3HT based hole-only devices and Electron-Hole motilities of P3HT:PCBM based electron-hole devices with and without CNT, measured using Molt-Gurney law.

Device	Electron motilities of PCBM based electron-only devices (μ_e) ($m^2 V^{-1} S^{-1}$)	Hole motilities of P3HT based hole-only devices (μ_h) ($m^2 V^{-1} S^{-1}$)	Electron-Hole motilities of P3HT:PCBM based electron-hole devices ($m^2 V^{-1} S^{-1}$)
Pure	x 10^{-6} 1.232	X 10^{-6} 6.695	1.87 x 10^{-5}
0.5%	9.593 x 10^{-6}	8.756X 10^{-6}	2.37 x 10^{-5}
1%	4.440 x 10^{-6}	3.766 X 10^{-6}	1.22 x 10^{-5}

noted for over 1% SWCNT concentrations, the hole mobility decreases, which also gives rise to inhibited carrier extraction. Consequently, with the increase in nanotube content to over 0.5%, there is a decrease in the photocurrent, which confirms the decrease in the number of extracted carriers [36].

Series Resistance and Shunt Resistances Characteristic of P3HT:PCBM:SWCNTs

The current-voltage property for SWCNT-doped with P3HT:PCBM is depicted in Table 4.

Extensive information was obtained for R_{sh} and R_s from the J-V curves figure and the series resistance (R_s) and shunt resistance (R_{sh}) was attained from the illumination of solar cells. Cell performance improved because of the considerable increase in fill factor (FF) and the open-circuit voltage (V_{oc}), as confirmed from the lesser Rs of the solar cells with the SWCNT doped P3HT:PCBM films. The V_{oc} increase is possibly due to the recovery of high shunt resistance because

Table 4. Important parameters of P3HT:PCBM and P3HT:PCBM:SWNT solar cells

Device	R_s (Ω cm^2)	R_{sh} (kΩ cm^2)
P3HT:PCBM	88.5	31.07
P3HT:PCBM:0.5wt%SWCNT	21.9	26.04
P3HT:PCBM: 1wt%SWCNT	56.7	27.01

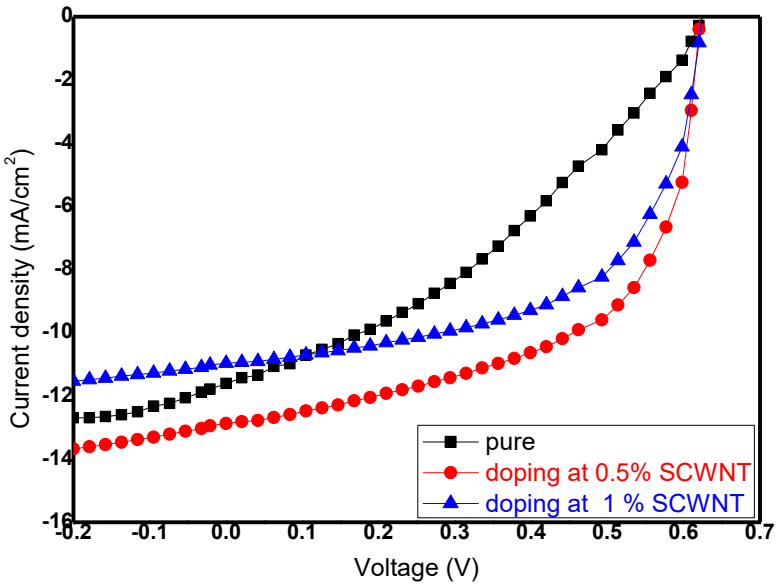

Fig. 7. I-V characteristic curves of solar cells are fabricated using P3HT:PCBM solar cell with and without SWCNTs incorporation.

Table 5. Photovoltaic performance of device with various SWCNTs concentrations.

Different doping (%)	V_{oc}	J_{sc}	FF	PCE
Pure	0.60	12.4	0.44	3.273
0.5	0.60	13.57	0.46	3.742
1	0.59	11.535	0.45	3.062

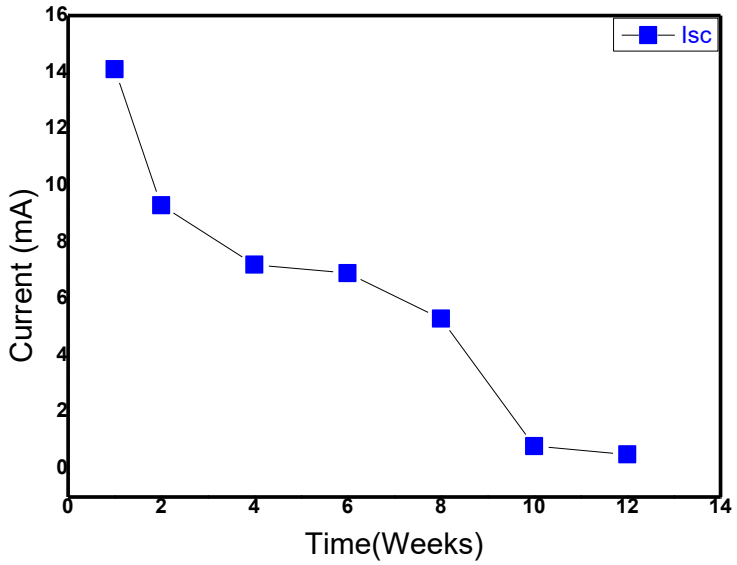

Fig. 8. Solar cell stability measurements of short circuit current measured over 12 weeks.

of the enhanced photovoltaic layer and electrode interface quality and the lower leakage current [34]. FF may increase because the series and the shunt resistance may improve because the photoactive layer has a rougher surface in comparison to the pure layer, and ultimately, to a decrease in the series resistance [35]. Hence, the FF values in the cells corresponds with P3HT:PCBM:SWCNTs layer. The FF was typically related to R_s as well as R_{sh}. FF for Organic photovoltaics (OPVs) may increase because of a reduction in Rs or an increase in Rsh. There are variations in the R_s values in cells with SWCNTs doped layer along with changes in the doping concentration [35]. The greatest values of FF and Voc were attained, which were consistent with the least Rs when the doping concentration was 0.5wt% of SWCNTs. The increase in V_{oc} of treated P3HT:PCBM leads to a lower R_s in the cells.

Current Density-Voltage (J-V) Measurements

The J-V properties of the ITO/V_2O_5/ P3HT: PCBM:SWCNTs/ TiO_2 /Au cells with SWCNTs %wt concentrations between 0% and 1% have been depicted in Fig. 7 and Table 5. Fig. 7 shows a representation of the reliance of SWCNT concentration on the main cell parameters of the device, e.g. power conversion efficiency, the short-circuit current density (J_{cs}), the open-circuit voltage (V_{oc}) and FF. It can be seen that all of the device parameters are affected by SWCNT doping.

For the undoped P3HT:PCBM cell, the Jsc is 12.4 mA cm^{-2}. After doping with SWCNTs, it achieves its highest value of 13.57 mA cm^{-2} at 0.5%, while at 1%, it decreases to 11.535 mA cm^{-2}. The V_{oc} is between 0.59 and 0.60, whereas it becomes 0.59V for higher concentrations (1 wt%). On the other hand, there is an increase in FF with increasing concentration of SWCNT, from 0.44 to 0.46. Thus, a highest efficiency of 3.742 was achieved for a SWCNT concentration of 0.5%. It is indicated that the increase in the photocurrent noted is essentially because of an increasingly efficient electron transport across the nanotube percolation pathways. There is dissociation of the photogenerated excitons at the P3HT:PCBM interfaces in the reference device and electrons move to the Au through hopping across the fullerenes. Including the nanotubes in the photoactive layer offers further routes for the electrons across the distributed carbon nanotube percolation network, inhibiting charge recombination and improving electron transport. It is believed that for greater SWCNTs concentrations, the photocurrent is restricted by higher recombination rate, and the effective mobility decreases because of the SWCNTs. The efficiency value that attained a highest at (2.87 mW/cm^2) was also noted by Shi-Hao [21]. The efficiency that attains its highest value at 1.4 mW/cm^2 was also identified by Emmanuel.

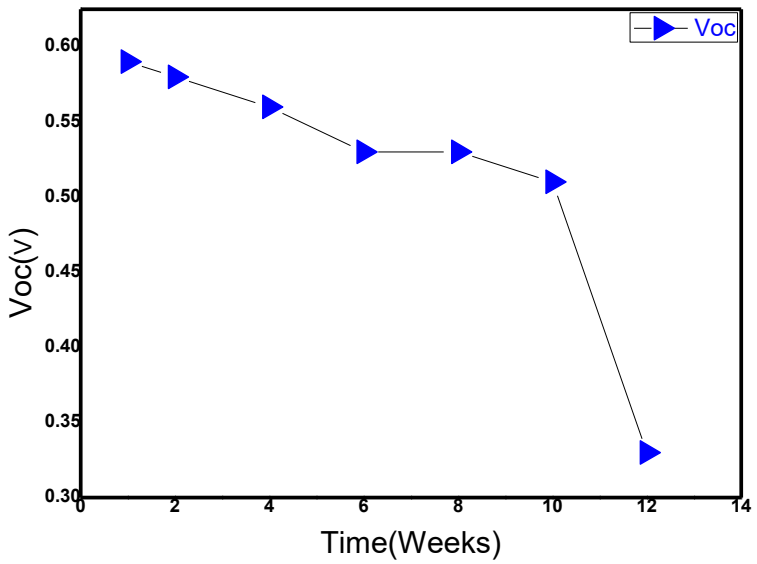

Fig. 9. Solar cell stability measurements of open circuit voltage measured over 12 weeks.

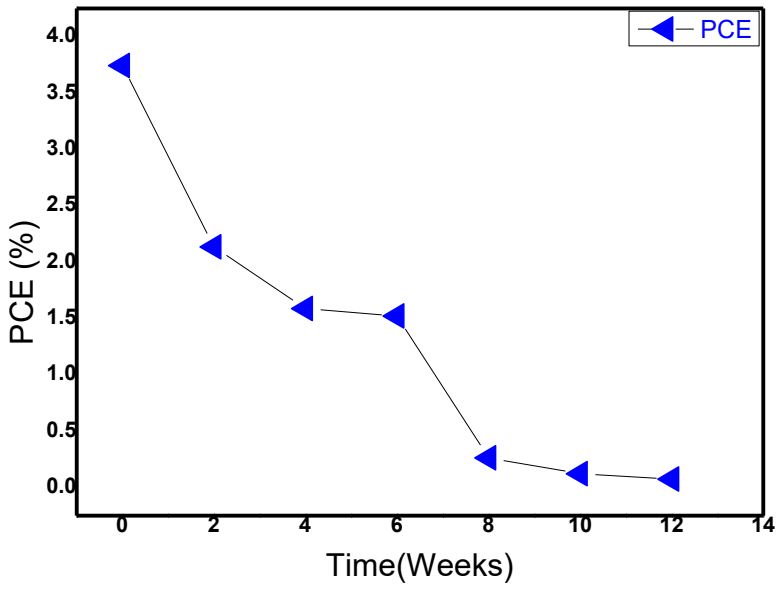

Fig. 10. Solar cell stability measurements of PCE measured over 12 weeks.

Furthermore, Hyung noted the efficiency that attains its greatest value at 4.1 mW/cm^2 [32].

Lifetime of Solar Cell Stability

It has achieved quite encouraging and consistent outcomes from an organic solar cell created using TiO_2 across a period of almost twelve weeks, as depicted in Figs. 8–10 shown below. There is a significantly more rapid decrease in the short circuit current in the initial two weeks; however, it becomes stable following the second week, after which light decreases. The open circuit voltage modifies light in the entire period over which the measures are taken.

There are several reasons for the degradation of solar cells, and the most widely accepted reason is that there is rapid activation of oxygen through UV illumination on the interface between metal oxides and the organics. If the thickness of the TiO_2 layer is not adequate enough to filter out all of the UV light, the organic compounds will then be aggressively attacked by the super-oxide or the hydrogen peroxide [36]. Apart from UV light, visible light is also partly absorbed by the thicker metal oxide layers, which decreases the ISC and PCE.

CONCLUSION

SWCNT improved the P3HT:PCBM:SWCNT devices performance by increasing the light-harvesting efficiency of the devices by increasing the rate of photon absorption. This proves that the SWCNT can be used as surface in organic bulk heterojunction organic solar cells devices, Because peak their extinction spectra matches with the peak of absorbance of P3HT:PCBM.

We have analyzed and optimized the various parameters such as, different doping SWCNT of P3HT:PCBM, which are important for improving the performance of the best device performance with different doping of P3HT:PCBM for 0.5% at SWCNT.

CONFLICT OF INTEREST

The authors declare that there is no conflict of interests regarding the publication of this manuscript.

REFERENCES

1. Cao W, Xue J. Recent progress in organic photovoltaics: device architecture and optical design. Energy & Environmental Science. 2014;7(7):2123.
2. Bhatia R, Kumar L. Functionalized carbon nanotube doping of P3HT:PCBM photovoltaic devices for enhancing short circuit current and efficiency. Journal of Saudi Chemical Society. 2017;21(3):366-376.
3. Morgan B, Dadmun MD. The role of incident light intensity, wavelength, and exposure time in the modification of conjugated polymer structure in solution. Eur Polym J. 2017;89:272-280.
4. Shi T, Gu L, Sun Y, Wang S, Zhang X, Zhu J, et al. A series of enzyme-controlled-release polymer-platinum-based drug

conjugates for the treatment of gastric cancer. Eur Polym J. 2017;92:105-116.
5. Cummins C, Flamant Q, Dwivedi R, Alvarez-Fernandez A, Demazy N, Bentaleb A, et al. An Ultra-Thin Near-Perfect Absorber via Block Copolymer Engineered Metasurfaces. Journal of Colloid and Interface Science. 2022;609:375-383.
6. Le Goupil F, Coin F, Pouriamanesh N, Fleury G, Hadziioannou G. Electrocaloric Enhancement Induced by Cocrystallization of Vinylidene Difluoride-Based Polymer Blends. ACS Macro Lett. 2021;10(12):1555-1562.
7. Palewicz M, Iwan A. Photovoltaic Phenomenon in Polymeric Thin Layer Solar Cells. Current Physical Chemistry. 2011;1(1):27-54.
8. Albrecht S, Janietz S, Schindler W, Frisch J, Kurpiers J, Kniepert J, et al. Fluorinated Copolymer PCPDTBT with Enhanced Open-Circuit Voltage and Reduced Recombination for Highly Efficient Polymer Solar Cells. Journal of the American Chemical Society. 2012;134(36):14932-14944.
9. Armin A, Wolfer P, Shaw PE, Hambsch M, Maasoumi F, Ullah M, et al. Simultaneous enhancement of charge generation quantum yield and carrier transport in organic solar cells. Journal of Materials Chemistry C. 2015;3(41):10799-10812.
10. Sadhu V, Nismy NA, Adikaari AADT, Henley SJ, Shkunov M, Silva SRP. The incorporation of mono- and bi-functionalized multiwall carbon nanotubes in organic photovoltaic cells. Nanotechnology. 2011;22(26):265607.
11. Chen R, Tang J, Yan Y, Liang Z. Solvent-Mediated n-Type Doping of SWCNTs to Achieve Superior Thermoelectric Power Factor. Advanced Materials Technologies. 2020:2000288.
12. Ahrenkiel RK, Dunlavy DJ. A new lifetime diagnostic system for photovoltaic materials. Sol Energy Mater Sol Cells. 2011;95(8):1985-1989.
13. Ren L, Wang S, Holtz M, Qiu J. The synergistic effect of nanocrystal integration and process optimization on solar cell efficiency. Nanotechnology. 2012;23(7):075401.
14. Kymakis E, Stylianakis MM, Spyropoulos GD, Stratakis E, Koudoumas E, Fotakis C. Spin coated carbon nanotubes as the hole transport layer in organic photovoltaics. Sol Energy Mater Sol Cells. 2012;96:298-301.
15. Capasso A, Salamandra L, Di Carlo A, Bell JM, Motta N. Low-temperature synthesis of carbon nanotubes on indium tin oxide electrodes for organic solar cells. Beilstein Journal of Nanotechnology. 2012;3:524-532.
16. Wu M-C, Lin Y-Y, Chen S, Liao H-C, Wu Y-J, Chen C-W, et al. Enhancing light absorption and carrier transport of P3HT by doping multi-wall carbon nanotubes. Chem Phys Lett. 2009;468(1-3):64-68.
17. Kettle J, Horie M, Majewski LA, Saunders BR, Tuladhar S, Nelson J, et al. Optimisation of PCPDTBT solar cells using polymer synthesis with Suzuki coupling. Sol Energy Mater Sol Cells. 2011;95(8):2186-2193.
18. Abuelwafa AA, Dongol M, El-Nahass MM, Soga T. Role of Platinum Octaethylporphyrin(PtOEP) in PCPDTBT: PCBM solar cell performance. J Mol Struct. 2020;1202:127303.
19. Stylianakis MM, Kymakis E. Efficiency enhancement of organic photovoltaics by addition of carbon nanotubes into both active and hole transport layer. Appl Phys Lett. 2012;100(9):093301.
20. Sai-Anand G, Dubey A, Gopalan A-I, Venkatesan S, Ruban S, Reza KM, et al. Additive assisted morphological optimization of photoactive layer in polymer solar cells. Sol Energy Mater Sol Cells. 2018;182:246-254.
21. Wang S-H, Hsiao Y-J, Fang T-H, Lin M-H, Kang S-H. Enhancing Performance and Nanomechanical Properties of Carbon Nanotube Doped P3HT:PCBM Solar Cells. ECS Journal of Solid State Science and Technology. 2013;2(11):M52-M55.
22. Veysel Tunc A, De Sio A, Riedel D, Deschler F, Da Como E, Parisi J, et al. Molecular doping of low-bandgap-polymer:fullerene solar cells: Effects on transport and solar cells. Org Electron. 2012;13(2):290-296.
23. Mallajosyula AT, Sundar Kumar Iyer S, Mazhari B. Role of single walled carbon nanotubes in improving the efficiency of P3HT:PCBM solar cells - impedance spectroscopy and morphology studies. 2010 35th IEEE Photovoltaic Specialists Conference; 2010/06: IEEE; 2010.
24. Derbal-Habak H, Bergeret C, Cousseau J, Nunzi JM. Improving the current density Jsc of organic solar cells P3HT:PCBM by structuring the photoactive layer with functionalized SWCNTs. Sol Energy Mater Sol Cells. 2011;95:S53-S56.
25. Derval-Habak H, Bergeret C, Cousseau J, Nunzi JM. Improving the efficiency of polymer solar cells by incorporation of functionalized SWCNTs in organic photovoltaic cells based on P3HT:PCBM photoactive layer. 2009 3rd ICTON Mediterranean Winter Conference (ICTON-MW); 2009/12: IEEE; 2009.
26. Geng J, Zeng T. Influence of Single-Walled Carbon Nanotubes Induced Crystallinity Enhancement and Morphology Change on Polymer Photovoltaic Devices. Journal of the American Chemical Society. 2006;128(51):16827-16833.
27. Jun GH, Jin SH, Park SH, Jeon S, Hong SH. Highly dispersed carbon nanotubes in organic media for polymer:fullerene photovoltaic devices. Carbon. 2012;50(1):40-46.
28. Musumeci AW, Silva GG, Liu J-W, Martens WN, Waclawik ER. Structure and conductivity of multi-walled carbon nanotube/poly(3-hexylthiophene) composite films. Polymer. 2007;48(6):1667-1678.
29. Dalton AB, Coleman JN, Panhuis Mih, McCarthy B, Drury A, Blau WJ, et al. Controlling the optical properties of a conjugated co-polymer through variation of backbone isomerism and the introduction of carbon nanotubes. J Photochem Photobiol A: Chem. 2001;144(1):31-41.
30. Ren S, Bernardi M, Lunt RR, Bulovic V, Grossman JC, Gradečak S. Toward Efficient Carbon Nanotube/P3HT Solar Cells: Active Layer Morphology, Electrical, and Optical Properties. Nano Lett. 2011;11(12):5316-5321.
31. Hyung Il P, Ju Min L, Ji Sun P, Sang Ouk K. Selective carrier transport enhancement in bulk-heterojunction organic photovoltaics with nitrogen or boron doped carbon nanotubes. 2011 IEEE Nanotechnology Materials and Devices Conference; 2011/10: IEEE; 2011.
32. Dai H. Carbon nanotubes: opportunities and challenges. Surface Science. 2002;500(1-3):218-241.
33. Mandoc MM, Koster LJA, Blom PWM. Optimum charge carrier mobility in organic solar cells. Appl Phys Lett. 2007;90(13):133504.
34. Kymakis E, Kornilios N, Koudoumas E. Carbon nanotube doping of P3HT : PCBM photovoltaic devices. J Phys D: Appl Phys. 2008;41(16):165110.
35. B. Sabti A, Y. Al-Luaibi M, A. Al-Fregi A. SYNTHESIS, CHARACTERIZATION, AND BIOLOGICAL ACTIVITY OF SOME NEW ORGANIC TELLURIIUM COMPOUNDS CONTAINING THIADIAZOLES. International Journal of Advanced Research. 2020;8(5):651-660.
36. van Eersel H, Janssen RAJ, Kemerink M. Mechanism for Efficient Photoinduced Charge Separation at Disordered Organic Heterointerfaces. Adv Funct Mater. 2012;22(13):2700-2708.